

Compensation of Sampling Frequency Offset With Digital Interpolation for OFDM-Based Visible Light Communication Systems

Qingqing Hu , Xianqing Jin , and Zhengyuan Xu , *Senior Member, IEEE*

Abstract—Compared with the traditional wireless communication systems, a visible light communication (VLC) system with intensity modulation and direct detection suffers nonlinearity and bandwidth-limitation of practical light emitting diodes (LEDs), which affect the synchronization and transmission performance of an orthogonal frequency division multiplexing signal. To improve the system spectral efficiency for relatively high capacity, an effective scheme for compensation of a sampling frequency offset (SFO) is required to achieve a high-signal-to-interference-plus-noise ratio (SINR). From the practical system design point of view, a fourth-order piecewise polynomial interpolator using the Farrow structure is proposed to digitally compensate SFO for the VLC systems. The LED nonlinearity causes extra high-frequency components in the signal spectrum, which may aggravate the aliasing effect when digital compensation of SFO is applied at the receiver. A theoretical study is, therefore, given to the impact of both the LED nonlinearity and SFO-induced intercarrier interference on the SINR based on a second-order polynomial nonlinear LED model. It is shown that the minimum required oversampling rate for achieving the maximum SINR using the fourth-order interpolator is reduced by approximately 15% and 50% compared to the second- and third-order interpolators, respectively. Both numerical and experimental results indicate that the proposed scheme can be used to effectively compensate a local oscillator frequency offset up to ± 1000 ppm at a minimum oversampling rate of 1.3 at the receiver.

Index Terms—Digital signal processing, light emitting diode, orthogonal frequency division multiplexing, sampling frequency offset, synchronization, visible light communication.

I. INTRODUCTION

VISIBLE light communication (VLC) has been considered as a promising technology for future high-speed and/or green communication systems [1]–[6] since it can address the

Manuscript received March 23, 2018; revised June 26, 2018 and September 1, 2018; accepted October 7, 2018. Date of publication October 15, 2018; date of current version November 2, 2018. This work was supported in part by the National Key Research and Development Program of China under Grant 2017YFB0403604; in part by the Key Program of National Natural Science Foundation of China under Grant 61631018; in part by the Key Research Program of Frontier Sciences of CAS under Grant QYZDY-SSW-JSC003; and in part by the Fundamental Research Funds for the Central Universities under Grant WK2100060022. (*Corresponding author: Xianqing Jin*)

The authors are with the Key Laboratory of Wireless-Optical Communications, Chinese Academy of Sciences, University of Science and Technology of China, Hefei 230026, China (e-mail: ruixhu@mail.ustc.edu.cn; xqjin@ustc.edu.cn; xuzy@ustc.edu.cn).

Color versions of one or more of the figures in this paper are available online at <http://ieeexplore.ieee.org>.

Digital Object Identifier 10.1109/JLT.2018.2876042

bandwidth challenge in the current wireless communication systems. In theory, VLC can offer a 1000 times greater bandwidth compared to the radio frequency (RF) communications [4]. In a cost-effective VLC system with commercially available white light emitting diodes (LEDs), intensity modulation/direct detection (IMDD) is preferable. However, the modulation bandwidth of the IMDD VLC systems is usually several MHz without optical filtering and equalization [5].

In order to improve signal spectral efficiency for high-speed VLC transmission, advanced modulation techniques including OFDM [3], [6] and carrier-less amplitude and phase (CAP) modulation [7] have been widely investigated in recent years. Both techniques can be used to mitigate the link bandwidth limitation effect by minimizing attenuation experienced on all subcarriers/sub-bands. Comparison between high-speed OFDM and multi-band CAP transceivers was reported in [8], which shows almost identical complexity of digital signal processing (DSP). In addition, for a large number of subcarriers/sub-bands, implementation of the inverse fast Fourier transform (IFFT)/FFT for OFDM is more efficient than the square-root raised cosine (SRRC) filters for multi-band CAP. Therefore, a small number of sub-bands is preferable for low-complexity multi-band CAP-based VLC systems, which however restricts the bandwidth flexibility. Owing to the adaptive bit and power loading on each subcarrier [3], [6], OFDM-based VLC systems have advantages of high spectral efficiency and flexible bandwidth/power allocation.

In an OFDM-based VLC system with high spectral efficiency, relatively precise synchronization is required since sampling frequency offset (SFO) introduces severe interference between adjacent OFDM subcarriers (inter-carrier interference, ICI) [9], [10]. SFO usually occurs due to mismatch of sampling clocks between the transmitter and receiver oscillators. In practice, the inherent instability of the transmitter and receiver oscillators causes clock frequency to fluctuate with time and temperature. In general, the clock frequency linearly increases with increasing temperature, which results in a typical frequency variation of 1.8% over an ambient temperature range from 0 °C to 85 °C [11]. Many standards for wireless communication systems specify an acceptable packet error rate for clocks with a tolerance of $\pm 20 \sim 25$ ppm [12]. In addition, the nonlinear transfer function (*P-U* curve) of LEDs causes extra new frequency components inside/outside the OFDM signal spectrum, which may affect the synchronization performance.

There are several different methods for the sampling frequency synchronization, which can be categorized in the following two types: 1) Synchronous mode: Sampling at the receiver can be synchronized to the symbol rate of the incoming signal with the feedback/feedforward information about estimated SFO for adjustment of the phase of a local clock [13]–[16]. Such a method has a large timing fluctuation due to high-level phase noise [17]. The receiver clock can also be synchronized by transmitting a dedicated clock signal along with information signal, which can be extracted at the receiver [18], [19]. However, this method requires additional analog circuits, which increases not only system complexity, but also peak-to-average power ratio (PAPR) of OFDM signal. 2) Asynchronous mode: Digital processing of the sampled signal at the receiver is applied to mitigate the SFO effect without altering the local clock. This can be realized by multiplying the signal after FFT (or before IFFT) with an exponential term derived from the estimated SFO to compensate phase error on each subcarrier at the receiver (or transmitter) [20]–[30], or interpolating the sampled signal to construct a resampled signal at the same sampling frequency as the transmitter [31]. For the former scheme of digital SFO compensation using the phase rotation correction term, the SFO effect can be partially mitigated because the ICI between subcarriers due to the SFO still exists. For the latter scheme using the digital interpolation, the ICI can be well alleviated in the digitally resampled signal so that the SFO effect is expected to be mitigated completely. In addition, the SFO compensation with the digital interpolation takes advantage of high-speed DSP, which has been widely used to mitigate the signal distortion effect in either optical wireless or fiber links in recent years. The sampling accuracy and/or speed requirement for digital-analog/analog-digital converters (DACs/ADCs) can thereby be relaxed with the scheme.

Compared with the traditional wireless communication systems, a VLC system with IMDD suffers nonlinearity and bandwidth-limitation of practical LEDs, which affect the OFDM synchronization performance. The motivation of this paper is to explore an effective synchronization scheme for the OFDM-VLC systems with high spectral efficiency. Investigation is focused on the digital compensation of SFO up to ± 1000 ppm by considering the LED nonlinearity and bandwidth-limitation. The impact of both the LED nonlinearity and SFO-induced ICI on signal to interference plus noise ratio (SINR) is theoretically investigated as the LED nonlinearity causes extra high frequency interference that may affect the performance of the digital SFO compensation. Therefore, an analytical expression for the theoretical SINR is derived for numerical evaluation. Along with the discussion about the SINR, a fourth-order piecewise polynomial interpolator using Farrow structure is proposed to digitally compensate SFO. The transmission performance of the OFDM-VLC systems employing the proposed scheme are numerically and experimentally investigated in a 6-m LED-based VLC link with a 3-dB bandwidth of approximately 6 MHz.

II. DIGITAL COMPENSATION OF SFO WITH A POLYNOMIAL INTERPOLATOR USING FARROW STRUCTURE

Fig. 1 shows a block diagram of a typical OFDM-based VLC system. At the transmitter, real-valued OFDM signal is

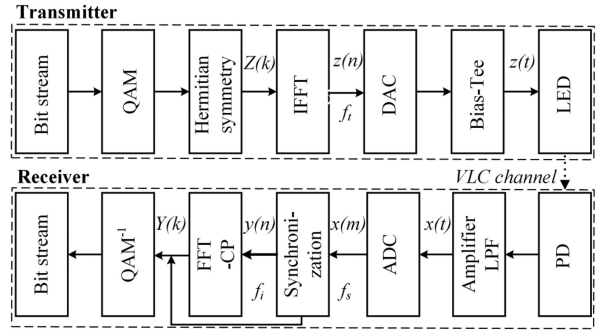


Fig. 1. A typical OFDM-based VLC system with an LED.

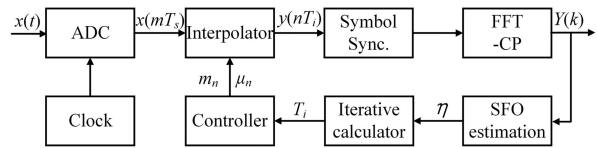


Fig. 2. Digital compensation of SFO with a polynomial interpolator.

generated with input data of IFFT satisfying Hermitian symmetry. After a DAC operating at a sampling frequency of $f_t = 1/T_t$, the analog OFDM signal is used to drive the LED with bias voltage for VLC transmission. Therefore, the transmitted signal is essentially DC biased optical OFDM (DCO-OFDM) signal. At the receiver, optical intensity of the received OFDM signal is detected with a photodiode (PD). The received electrical OFDM signal is then digitized with an ADC at a sampling frequency of f_s before signal recovery in DSP including synchronization, FFT and equalization. Given the instability of the transmitter/receiver oscillators, the frequency of the receiver clock is defined as $f_s = 1/T_s = \lambda f_t (1 + \eta)$, where λ is oversampling rate and η is SFO. The SFO is digitally compensated as shown in Fig. 2. In this section, theoretical investigation is given to the proposed digital compensation of SFO with a polynomial interpolator using Farrow structure. The SINR due to the SFO-induced ICI and LED nonlinearity is also analytically studied.

A. Sampling Frequency Offset (SFO)

For simplicity of analysis of the SFO effect, a linear channel is initially assumed. The demodulated OFDM signal at the k th subcarrier of the l th OFDM symbol is written as [9]

$$\begin{aligned}
Y_l(k) &= e^{j\pi k\eta(N-1+2IN_s+2N_g)/N} \cdot \frac{\sin(\pi\eta k) \cdot Z_l(k) H_l(k)}{N \sin(\pi\eta k/N)} \\
&+ \sum_{i=0, i \neq k}^{N-1} e^{j\pi[(i-k+i\eta)(N-1)+2i\eta(lN_s+N_g)]/N} \\
&\cdot \frac{\sin(\pi(i+i\eta-k)) \cdot Z_l(i) H_l(i)}{N \sin(\pi(i+i\eta-k)/N)} + n_l(k) \quad (1)
\end{aligned}$$

where N and N_g are size of inverse FFT (IFFT) and cyclic prefix, respectively. The symbol length N_s is thereby equal to $(N + N_g)$. Z_l and H_l are transmitted OFDM signal and frequency response of the VLC channel, respectively. n_l is complex noise. As seen from Eq. (1), the SFO causes amplitude attenuation, phase

rotation and ICI. Before the digital SFO compensation, the SFO is estimated with scattered pilots after FFT [28]. The phase rotation of the k th pilot subcarrier in the l th OFDM symbol is given by $\varphi_{l,k} = \pi k \eta (2lN_s + 2N_g + N - 1)/N$. With the phase difference of pilots between two OFDM symbols delayed by D symbols (pilot period), $\vec{\theta}_{l,k} = \vec{\varphi}_{l,k} - \vec{\varphi}_{l-D,k} = 2\pi N_s D \eta k/N$, the estimated SFO, $\hat{\eta}$, is obtained with ($L-D$) symbols

$$\hat{\eta} = \hat{A}N/(2\pi N_s D) \quad (2)$$

$$\hat{A} = \sum_{l=D+1}^L \sum_{i=1}^p k_i \theta_{l,k_i} / (L-D) \sum_{i=1}^p k_i^2 \quad (3)$$

where k_i is pilot index, and L is the number of OFDM symbols used to average the estimated SFO. In Fig. 2, a feedback loop is applied to track SFO at a resampling frequency given below

$$f_i = 1/T_i = f'_i / (1 + \hat{\eta}) \quad (4)$$

where f'_i is the calculated resampling frequency in the previous loop and its initial value is f_s/λ .

B. Digital Compensation of SFO

With the estimated SFO, a piecewise polynomial interpolator with Farrow structure is used to construct a resampled signal [31], [32],

$$y(nT_i) = \sum_m x(mT_s) h_I(nT_i - mT_s) \quad (5)$$

where h_I is impulse response of the digital interpolator. The advantage of the polynomial interpolator is that the interpolated signal can be obtained without storing samples for calculation of impulse responses. With the polynomial interpolation using Farrow structure for high-speed systems, Eq. (5) can be derived in the following form [31], [32],

$$\begin{aligned} y(nT_i) &= y((m_n + \mu_n)T_s) \\ &= \sum_{i=I_1}^{I_2} x[(m_n - i)T_s] h_I[(i + \mu_n)T_s] \\ &= \sum_{i=I_1}^{I_2} x[(m_n - i)T_s] \sum_{q=0}^Q c_q(i) \mu_n^q \end{aligned} \quad (6)$$

where $m_n = \text{int}[nT_i/T_s]$, $\mu_n = nT_i/T_s - m_n$. $c_q(i)$ is coefficients of the interpolation filter. The operator $\text{int}[x]$ means the largest integer not exceeding x . Here, a fourth-order piecewise polynomial interpolator ($Q = 4$) using Farrow structure is proposed to improve the VLC transmission performance. As shown in Fig. 3(a), it can suppress the spectral artifacts more than 60 dB below the designed passband [33]. To verify the improved transmission performance, the piecewise-parabolic ($Q = 2$) and cubic ($Q = 3$) interpolation filters are also investigated. Compared with the 2nd (piecewise-parabolic) and 3rd (cubic) order interpolators [32], [33], the spectrum of the 4th order interpolator is flatter when $fT_t < 0.5$, but attenuated more when $fT_t \geq 0.5$.

The controller in Fig. 2 is designed to calculate integer index m_n and fractional interval μ_n for the input of the interpolator

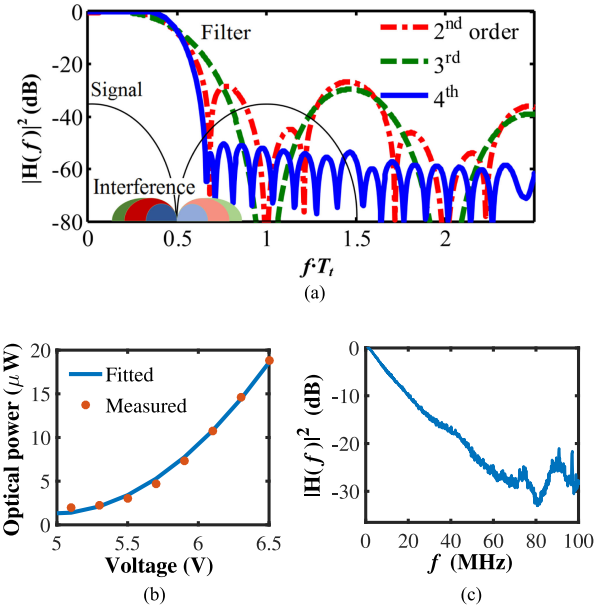


Fig. 3. (a) Spectra of interpolation filters using Farrow structure and the aliasing effect ($\lambda = 1.0$), signal bandwidth: $1/(2T_t)$, (b) Measured/fitted $P-U$ curve of the LED, (c) Frequency response of the LED-based VLC link.

with the calculated T_i from the iterative calculator:

$$\begin{aligned} m_{n+1} &= m_n + \text{int} \left[\mu_n + \frac{T_i}{T_s} \right] \\ \mu_{n+1} &= \left(\mu_n + \frac{T_i}{T_s} \right) - \text{int} \left[\mu_n + \frac{T_i}{T_s} \right], \end{aligned} \quad (7)$$

C. SINR Due to SFO-Induced ICI and LED Nonlinearity

To focus on theoretical investigation of the SFO compensation, an ideal DAC is assumed. At the transmitter, the LED is driven by an electrical OFDM signal $z(t)$:

$$z(t) = V_b + \frac{u}{2} \left[\sum_{k=1}^{N/2-1} Z(k) e^{j2\pi k \Delta f t} + \sum_{k=1}^{N/2-1} Z^*(k) e^{-j2\pi k \Delta f t} \right] \quad (8)$$

where V_b and u are bias voltage and electrical gain, respectively. Δf is subcarrier spacing, which is equal to f_t/N . The operator $*$ represents the conjugate operator.

To model the LED nonlinearity, a second-order polynomial form is used to mimic the measured transfer function ($P-U$ curve) of the LED as shown in Fig. 3(b), whilst Fig. 3(c) shows frequency response of the LED-based VLC link. The intensity of the optical signal from the LED is then written as [34]

$$p(t) = b_2 z^2(t) + b_1 z(t) + b_0 \quad (9)$$

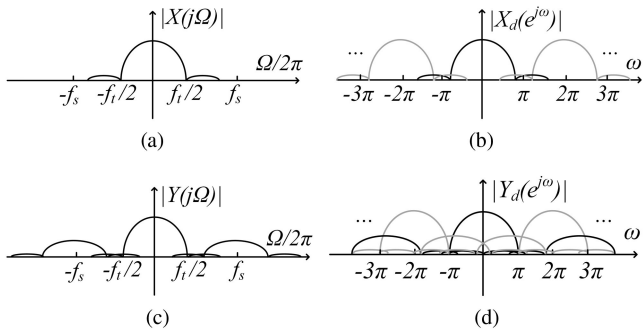


Fig. 4. Spectra of signals (a) $x(t)$, (b) $x(m)$, (c) $y(t)$, (d) $y(n)$. $\Omega = 2\pi f = \omega/T$.

In the frequency domain, Eq. (9) can be derived as

$$P(k\Delta f) = \begin{cases} \frac{u(b_1 + 2b_2 V_b)}{2} Z(k) + \frac{u^2 b_2}{4} [\sum_{T_k} Z(m)Z(l) \\ + 2 \sum_{\Lambda_k} Z(m)Z^*(l)], & k \in (0, N/2 - 1] \\ \frac{u^2 b_2}{4} \sum_{G_k} Z(m)Z(l), & k \in [N/2, N - 1] \end{cases}$$

$$(G_k, T_k) = \{m, l | 1 \leq m, l \leq N/2 - 1 \text{ } \& \text{ } (m + l) = k\}$$

$$\Lambda_k = \{m, l | 1 \leq m, l \leq N/2 - 1 \text{ } \& \text{ } (m - l) = k\}$$
(10)

At the receiver, the optical intensity of the OFDM signal is linearly converted into electrical current. After the electrical amplifier and LPF, the spectrum of the continuous signal $x(t)$ as shown in Fig. 4(a) can be expressed as

$$X(j\Omega) = P(j\Omega)H_c(j\Omega) + n(j\Omega) \quad (11)$$

where $\Omega = 2\pi f$. H_c is frequency response of the VLC link including the LED, PD, electrical amplifier and LPF. $P(j\Omega)$ is spectrum of the optical intensity signal after the LED, which can be easily derived from Eq. (10). $n(j\Omega)$ is spectrum of sum of time-domain shot noise and thermal noise at the receiver. For simplicity, the time-domain noise is modeled as additive white Gaussian noise (AWGN) with a variance of σ_n^2 [35]. $n(j\Omega)$ thus satisfies complex Gaussian distribution. The LPF is used to partially suppress interferences outside the signal spectrum. The spectrum of $x(m)$ after ADC in Fig. 4(b) is expressed as

$$X_d(e^{j\omega}) = f_s \sum_{r=-\infty}^{\infty} X(j\omega f_s + j2\pi r f_s) \quad (12)$$

where r is an integer number, and $\omega = \Omega/f_s$. The oversampling rate λ of $1 \sim 2$ at the receiver ADC ($f_s \in [f_t, 2f_t]$) is considered here. As the first sidelobe of the signal spectrum $X(j\Omega)$ contains most power of out-of-band signal, the spectrum of the continuous-time signal reconstructed with interpolation in Fig. 4(c) is calculated as follows

$$Y(j\Omega) = H_I(j\Omega) \sum_{r=-1}^1 X(j\Omega + j2\pi r f_s) \quad (13)$$

where $H_I(j\Omega)$ is spectrum of the interpolation filter. In Fig. 4(d), the spectrum of the resampled signal $y(n)$ can be derived as

$$Y_d(e^{j\omega}) = f_i \sum_{r_2=-\infty}^{\infty} H_I(j\omega f_i + j2\pi r_2 f_i) \sum_{r_1=-1}^1 X(j\omega f_i + j2\pi r_2 f_i + j2\pi r_1 f_s). \quad (14)$$

If SFO is accurately estimated, $f_i \approx f_t$ is satisfied. Combining Eqs. (10)–(14), the signal after FFT can be written as

$$Y(k) = f_i [H(k)Z(k) + I(k) + n_F(k)] \quad (15)$$

$$H(k) = \frac{u(b_1 + 2b_2 V_b)}{2} H_c(k)H_I(k) \quad (16)$$

$$I(k) = \sum_{i=1}^2 [P(k + (\psi - i)N)H_c(k + (\psi - i)N)H_I(k - iN) \\ + P(k - (\psi - i)N)H_c(k - (\psi - i)N)H_I(k + iN)] \\ + \frac{u^2 b_2}{4} \left[\sum_{T_k} Z(m)Z(l) + 2 \sum_{\Lambda_k} Z(m)Z^*(l) \right] \\ \times H_c(k)H_I(k) \quad (17)$$

$$n_F(k) = \sum_{i=1}^2 [n(k + (\psi - i)N)H_I(k - iN) \\ + n(k - (\psi - i)N)H_I(k + iN)] + n(k)H_I(k) \quad (18)$$

where $\psi = \lambda(1 + \eta)$. H is system frequency response. I indicates ICI due to the LED nonlinearity and SFO. n_F is received noise after the SFO compensation in the frequency domain. Therefore, the SINR on the k th subcarrier is obtained as

$$SINR_k = \frac{|H(k)|^2 E(|Z(k)|^2)}{E(|I(k)|^2) + E(|n_F(k)|^2)} \quad (19)$$

where the operator $E()$ represents the expectation operator. As shown in Eqs. (15)–(19), SINR depends on SFO, oversampling rate at the receiver, frequency responses of the polynomial interpolators and VLC channel, and LED nonlinearity, which are discussed in Section III.

III. NUMERICAL VERIFICATION OF THE DIGITAL SFO COMPENSATION

Based on the theoretical study of the SFO effect in the OFDM-based VLC system in the previous section, 16-QAM-OFDM transmission performance is numerically investigated for verification of the proposed digital compensation of SFO. To distinguish the LED nonlinearity effect from the other, simulation of the OFDM transmission in the AWGN and VLC channels is carried out in Matlab. For the AWGN channel, a linear LED is assumed, whilst for the VLC channel the nonlinear LED is modelled with Eq. (9) [36]. A good agreement between the measured and simulated $P-U$ curves of the LED is observed in Fig. 3(b). According to the signal procedure in Fig. 1, the

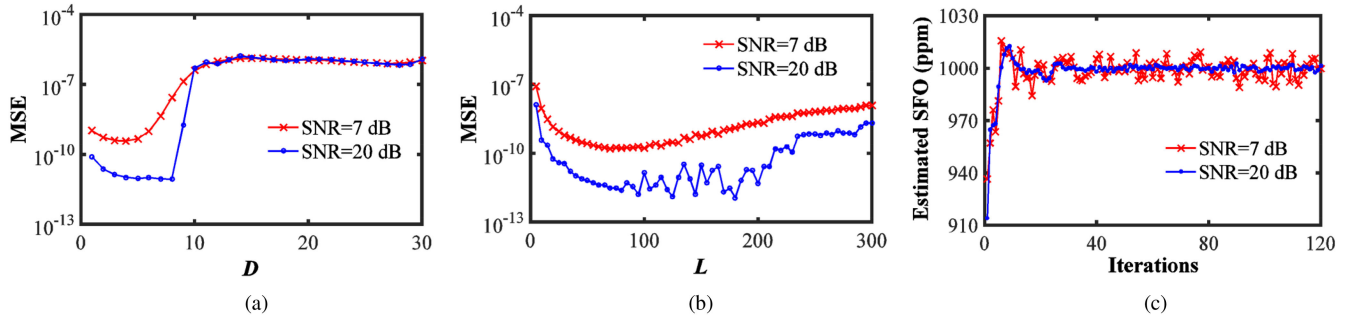


Fig. 5. MSE as a function of (a) D ($L = 40$) or (b) L ($D = 4$) and (c) Estimated SFO versus iterations ($L \leq 40$, $D = 4$) under AWGN. SFO = 1000 ppm. $\lambda = 1.0$.

received OFDM signal is digitally recovered with the following parameters: As the increment of the number of subcarriers or IFFT size would cause not only high PAPR but also increased DSP complexity, a typical value of 128 is adopted for the IFFT size. To avoid inter-symbol-interference (ISI), the CP length is set to 16, which corresponds to $0.64 \mu\text{s}$ at a sampling rate of 25 MHz. The CP period is larger than the inverse of the LED bandwidth ($0.17 \mu\text{s}$). Pilots on the 12th, 23rd, 34th, and 45th subcarriers are used to estimate SFO. The sampling frequency of DAC is fixed at 25 MHz, whilst the bandwidth of OFDM signal is 12.5 MHz. At the receiver, an ideal electrical LPF is applied to not only suppress interferences outside the signal spectrum, but also isolate the aliasing effect due to the LPF for a fair comparison in improved error vector magnitude (EVM) performance between simulation and experiment.

Prior to investigation of the OFDM transmission performance, key parameters of D (pilot period) and L (number of symbols for SFO estimation) from Eqs. (2)–(3) are optimized under AWGN in Fig. 5, where $SFO = 1000$ ppm, $\lambda = 1.0$. Mean square error (MSE) of the estimated SFO is used to quantify the estimation performance. As seen in Fig. 5, the increment of MSE with increasing L or D for a signal-to-noise ratio (SNR) of 7 dB or 20 dB when $L \geq 40$ or $D \geq 4$ is observed. This is because the estimated phase difference between two pilot symbols exceeds the range $[-\pi, \pi]$, or the start of the drifted FFT window due to the SFO exceeds the cyclic prefix range. For $L < 40$ or $D < 4$, the MSE performance degrades with decreasing L or D due to the receiver noise. It is noted that the optimum D and L values ($D = 4$, $L = 40$) at minimum MSE of estimated SFO are less than the theoretical up-limit, $D < N/(2N_s K_p |\eta|)$ and $L < N_g/(\eta N_s)$, where K_p is the largest index of pilot subcarriers. This can be explained by the phase noise for the optimum D and limited LED bandwidth for the optimum L . As an example, Fig. 5(c) shows estimated SFO as a function of iterations when $L \leq 40$ and $D = 4$. Due to the noise effect, a relatively large fluctuation in the estimated SFO is observed for SNR = 7 dB compared with SNR = 20 dB. It is clear to see that the estimated SFO converges at the real SFO of 1000 ppm when the number of iterations is larger than or equal to 40. Therefore, the optimized parameters of $L = 40$ and $D = 4$ are used in the following investigations.

After the optimization of key parameters, investigation of EVM and SINR performances in the AWGN or VLC channel is conducted to validate the performance of the digital SFO com-

pensation in Fig. 6, where SFO = 100 ppm and SNR = 28 dB. For the VLC channel, the characteristics of the LED are shown in Fig. 3(b) and (c). As seen in Fig. 6, the 4th order polynomial interpolator outperforms the 2nd and 3rd order polynomial interpolators at an oversampling rate of 1 or 1.5. The EVM calculated with a training sequence is almost consistent with the SINR calculated from Eq. (19). Fig. 6(a) and (b) shows a significantly degraded EVM performance on the high frequency subcarriers for both cases when $\lambda = 1.0$. This is because the imperfect interpolation filter causes out-of-band signal, which interferes the signal on the high-frequency subcarriers during the resampling process as shown in Fig. 3(a). Such interference can be alleviated by oversampling the received signal at a relatively high frequency. This is confirmed in Fig. 6(c) and (d) that the interference on the high-frequency subcarriers disappears when $\lambda = 1.5$.

In Fig. 6(c), the EVM performance under AWGN on the low-frequency subcarriers degrades by up to approximately 3 dB and 10 dB for the 2nd and 3rd order polynomial interpolators, respectively. However, for the 4th order polynomial interpolator, the EVM on each subcarrier is around -28 dB in the AWGN channel, which indicates a negligible power penalty. This is explained by the fact that the generated image component in the low-frequency region for the 4th order polynomial interpolator is depressed more than that for the 2nd and 3rd order polynomial interpolators as shown in Fig. 7(a). It is noted that the minimum EVM in the AWGN channel is approximately 6 dB lower than that in the VLC channel, which is limited by the LED nonlinearity induced crosstalk. The signal-to-crosstalk ratio (SXR) can be calculated from Eq. (10). In Fig. 7(b) the calculated SXR linearly increases with subcarrier index. The maximum variation of approximately 3 dB in SXR agrees well with the result in [34].

By varying the receiver sampling frequency, f_s , under the same condition as Fig. 6, the impact of oversampling rate on SINR performance is shown in Fig. 8. For both the AWGN and VLC channel cases, the SINR is improved by increasing oversampling rate until the maximum SINR is achieved. The minimum required oversampling rate for the best SINR performance using the 4th order interpolator is approximately equal to 1.3, which is smaller than the 2nd or 3rd order interpolator. Due to orthogonality between adjacent OFDM subcarriers, there is a fluctuation of <1.3 dB (<0.3 dB) in SINR in the AWGN (VLC) channel as seen in the inset. Such fluctuation occurs for a relatively high oversampling rate. As an example,

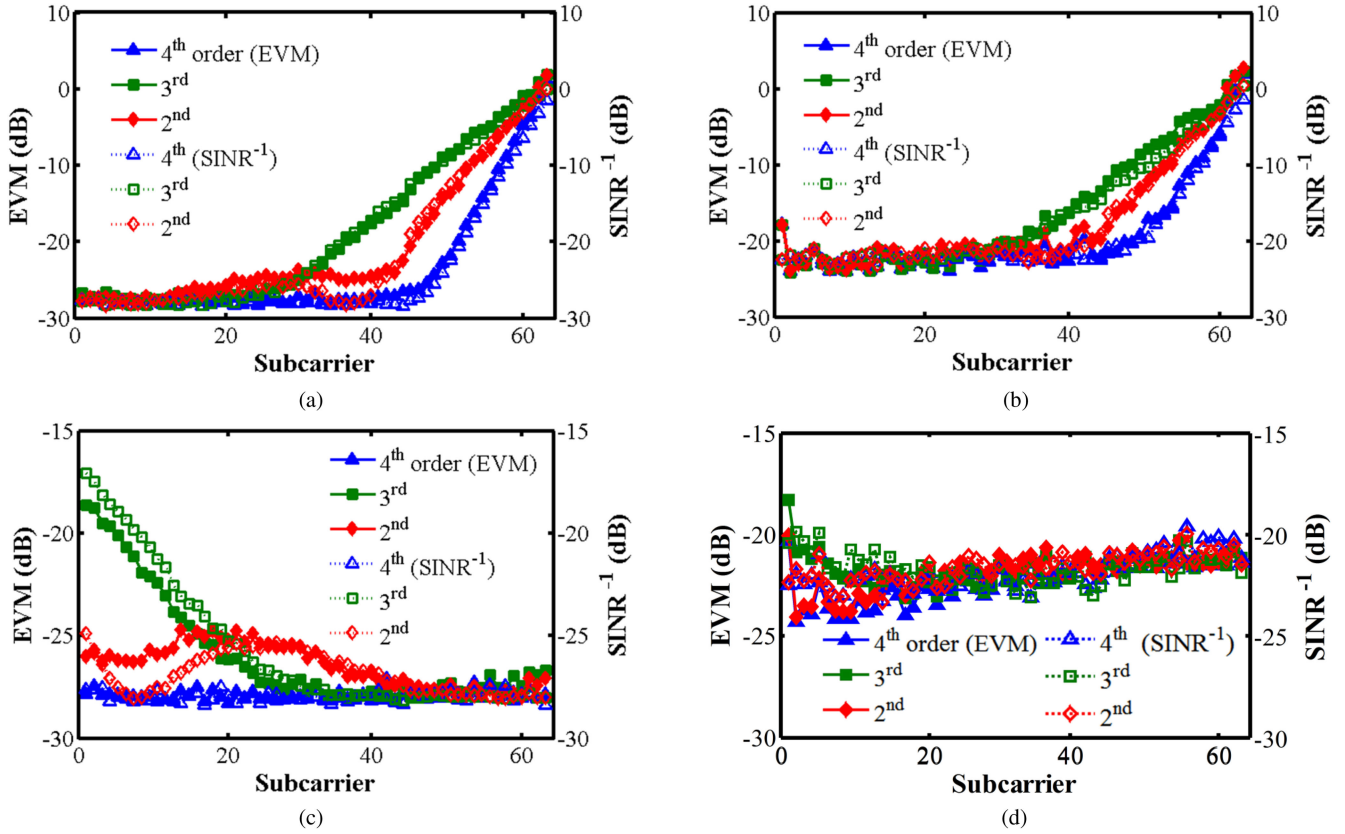


Fig. 6. EVM and SINR performances in the AWGN (a, c) or VLC (b, d) channel at an oversampling rate of (a, b) $\lambda = 1$, (c, d) $\lambda = 1.5$. SNR = 28 dB, SFO = 100 ppm.

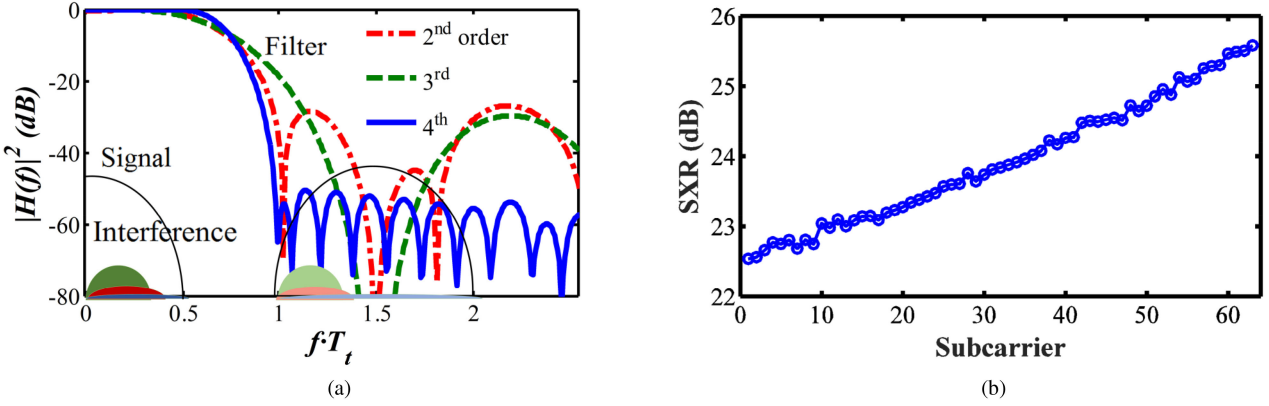
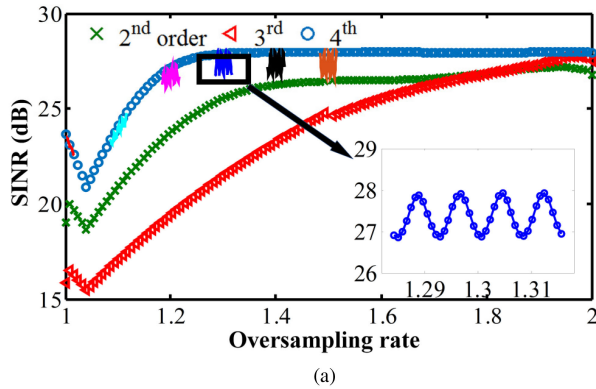


Fig. 7. (a) Aliasing effect under AWGN when $\lambda = 1.5$. Shade area represents image components. (b) SXR distribution in the VLC channel. SFO = 100 ppm.

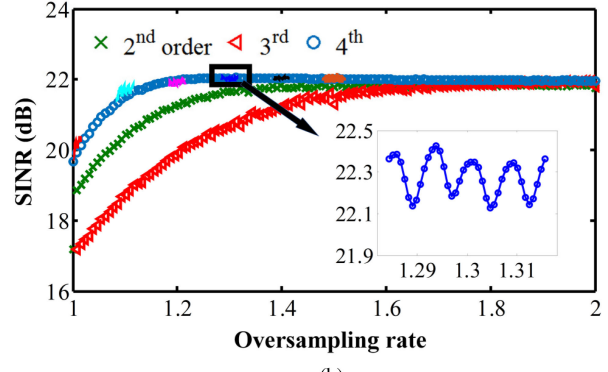
SINRs at the oversampling rates of around 1.0, 1.1, 1.2, 1.3, 1.4 and 1.5 are plotted in Fig. 8, where the step size of λ is $\Delta f/10$. The relatively small fluctuation of SINR for the VLC channel is due to the LED nonlinearity induced crosstalk between different subcarriers. Therefore, the receiver sampling frequency is usually set equal to multiple subcarrier spaces for calculation of SINR in Fig. 8. It is noted that for the AWGN channel, there is a SINR dip at $\lambda \approx 1.04$ because of the shape decrease in the filter responses near the signal bandwidth as seen in Fig. 3(a).

To investigate the impact of SFO on the EVM performance, Fig. 9 shows EVM performance as a function of SFO at different

oversampling rates from 1.0 to 2.0. For the perfect sampling case when SFO = 0 and $\lambda = 1$, the EVM values calculated with different interpolators are -28 dB and -22 dB in the AWGN and VLC channels, respectively. However, the EVM performance sharply degrades with increasing absolute value of SFO due to aliasing effect. This indicates that the EVM performance of the OFDM signal is sensitive to SFO. By increasing oversampling rate, the EVM for $\lambda = 1.3$ or 2 reaches minimum in either the AWGN or VLC channel. The 4th order interpolator always performs better than the 2nd and 3rd interpolators, which agrees very well with the results in Fig. 6. It is noted that the EVM for

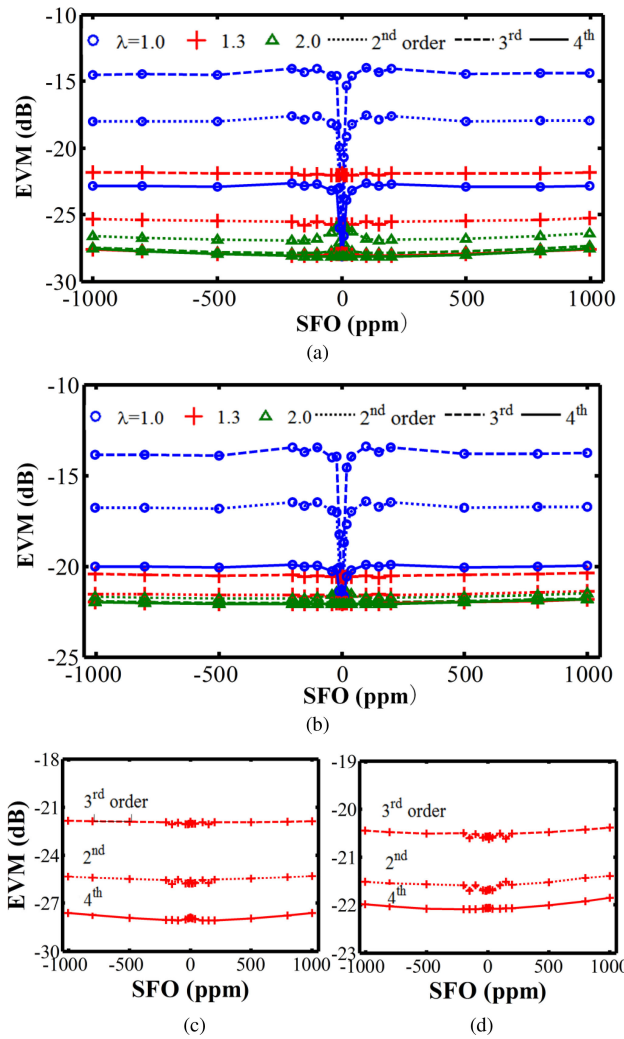


(a)



(b)

Fig. 8. SINR versus oversampling rate in the (a) AWGN or (b) VLC channel, SFO = 100 ppm.

Fig. 9. EVM versus SFO at different oversampling rates in the (a, c) AWGN or (b, d) VLC channel. (c, d): $\lambda = 1.3$.

$\lambda = 1.3$ reaches the best performance as the same as that for $\lambda = 2.0$ for $|SFO| \leq 1000$ ppm, whilst the EVM for the 4th order interpolator remains almost constant for different SFO values. As seen in Fig. 9(c) and (d), the EVM curves for different interpolators when $\lambda = 1.3$ are parallel to each other. Compared

TABLE I
COMPUTATIONAL COMPLEXITY OF DIFFERENT INTERPOLATORS [32], [33]

Operation	2 nd	3 rd	4 th
Delay	5	8	7
Scale by constant	1	3	40
Add/Subtract	9	11	39
Multiply/Divide	2	3	4

with the 2nd and 3rd order interpolators, the EVM achieved with the 4th order interpolator in the VLC or AWGN channel is improved by more than 0.5 dB or 2.5 dB.

Table I shows the computational complexity of different interpolators in terms of numbers of different operations required to calculate one interpolant [32], [33]. Because the scale by constant for the 4th order interpolator is 40, the number of operations (add/subtract/multiply/divide) for the 4th order interpolator is about 3 times that for the 3rd order interpolator. In addition, the proposed 4th order piecewise polynomial interpolator using Farrow structure is essentially based on a finite impulse response (FIR) filter as described in Eq. (6). The FIR filters widely used for channel equalization in a single carrier system can be easily developed for the proposed digital solution in a real-time system for practical OFDM-VLC applications.

IV. EXPERIMENTAL RESULTS AND DISCUSSION

After the numerical verification of the proposed scheme for the digital SFO compensation, experimental investigation of the EVM performance of 16-QAM-OFDM signal is conducted over a 6-m LED-based VLC link. The 3-dB bandwidth of the LED is approximately 6 MHz. The experimental setup of the VLC system is depicted in Fig. 10. Independent clocks are applied to introduce SFO between the arbitrary waveform generator (AWG) at the transmitter and digital storage oscilloscope (DSO) at the receiver. Parameters for the numerical study in Section III are adopted for signal generation/recovery except those listed in Table II due to discrete values of sampling clocks at the AWG or DSO.

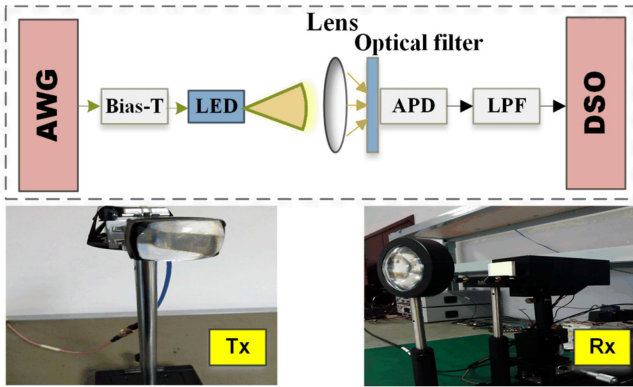


Fig. 10. Experimental setup of a LED-based VLC system.

TABLE II
PARAMETERS OF DSO AND OFDM SIGNAL

Oversampling rate, λ	f_s of DSO (MHz)	Signal bandwidth (MHz)	Bit rate (Mb/s)
1.0	25	12.5	43.8
1.3	25	9.6	33.7
1.5	25	8.3	29.2
1.7	25	7.4	25.7
2.0	50	12.5	43.8

At the transmitter, a 5×10^5 -bit pseudo random binary sequence is generated for 16-QAM mapping. Every 40 OFDM symbols form a data block for the SFO estimation. To identify start position of the FFT window and the whole sequence, 4 training symbols are inserted at the beginning of the OFDM sequence for symbol synchronization. The OFDM signal generated with Matlab is loaded into the AWG (Tektronix 5014C, 14-bit DAC). The electrical OFDM signal from the AWG is used to drive the LED with a Bias-Tee (ZFBT6GW-FT+). The Bias voltage of the LED is 5.75 V, and the peak-to-peak voltage of the driving signal is 0.4 V [36]. At the receiver, a lens with a diameter of 10 cm is placed in front of the avalanche photodiode (APD) to collect light for a high optical gain. The light passing through a blue filter is then detected by the APD. After an electrical LPF, the received signal is sampled by a digital storage oscilloscope (DSO, Agilent MSO-X 6004A, 12-bit ADC) for offline signal recovery. To further reduce the noise and interference beyond the signal spectrum, an ideal digital LPF is applied before the digital SFO compensation. The output of the 10 MHz reference clock of the AWG is connected to the input of DSO in order to introduce a precise SFO, which is varied by adjusting the sampling frequency of the AWG.

As shown in Fig. 11(a) and (b), the constellations of the received 16-QAM-OFDM signal for relatively large SFO before the SFO compensation are rotated and dispersed due to the SFO-induced ICI, crosstalk and receiver noise. In Fig. 11(d), the constellation after the SFO compensation with the 4th order interpolator is significantly improved, which is similar to that for SFO = 0 in Fig. 11(c). This indicates the effectiveness of the SFO compensation with the proposed scheme.

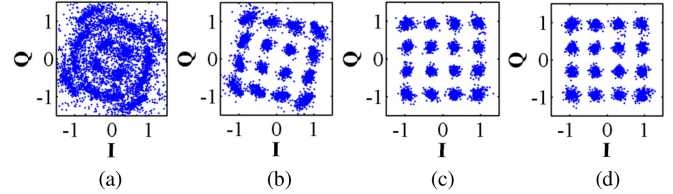
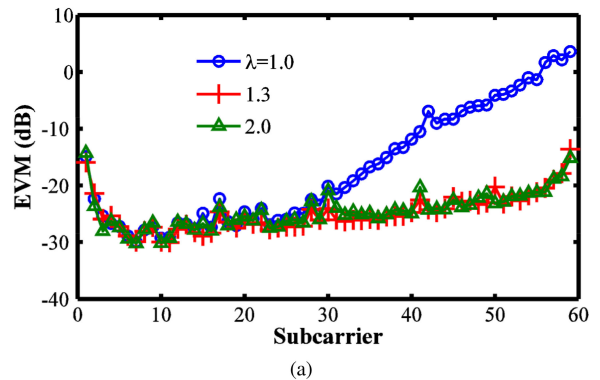
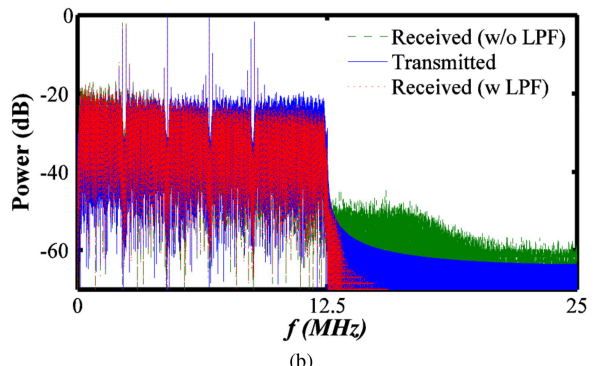


Fig. 11. Constellations of the received 16-QAM-OFDM signal (a)–(c) before or (d) after SFO compensation. (a)–(c) SFO = 80, 40, 0 ppm, (d) SFO = 80 ppm.



(a)



(b)

Fig. 12. (a) EVM performance with the 4th order interpolator, SFO = 100 ppm. (b) Power spectra of the transmitted signal and received signal with (w) or without (w/o) digital LPF.

Fig. 12(a) shows EVM performance on each subcarrier using the 4th order interpolator. When $\lambda = 1.0$, the EVM starts to sharply degrade from the 30th to the last subcarrier. Such trend is the same as that in Fig. 6(b). The relatively high EVM on subcarriers 1–3 is because of the low frequency distortion of electrical components (Bias-Tee) in the VLC link. From the comparison between power spectra of the transmitted and received signals in Fig. 12(b), the LED nonlinearity induced extra high frequency components are observed, which is about 25 dB lower than the power of the last subcarrier. The measured nonlinearity-induced interference agrees well with the calculated SXR in Fig. 7(b). Owing to the imperfect electrical LPF with a 3-dB cut-off frequency of 10 MHz (or 15 MHz) for $\lambda = 1.3$ (or 2.0), the new frequency components beyond the signal bandwidth (12.5 MHz) cause interference on OFDM subcarriers. Therefore, the EVM for $\lambda = 1.3$ (or 2.0) slowly degrades with subcarrier index in Fig. 12(a).

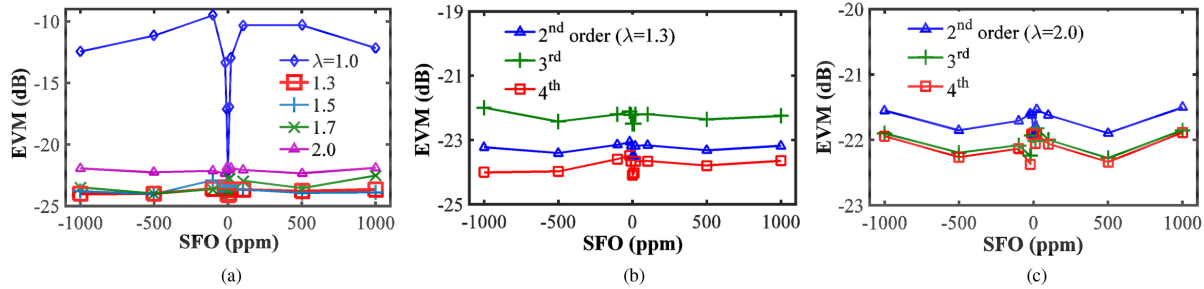


Fig. 13. (a) Measured EVM versus SFO (the 4th order interpolator). (b, c) EVM performance with the 2nd, 3rd and 4th order interpolators when $\lambda = 1.3$ (b), 2.0 (c).

To gain a better understanding of the performance of the digital SFO compensation, Fig. 13(a) shows the measured EVM at different oversampling rates with the 4th order interpolator. The best EVM of approximately -24 dB is achieved at an oversampling rate of ≥ 1.3 , which confirms the theoretical prediction in Figs. 8 and 9. The slight variation in EVM for $\lambda \geq 1.3$ is due to different bandwidth of the OFDM signals in the experiment. Since the signal with relatively small bandwidth attenuates less than that with relatively large bandwidth, the EVM for $\lambda = 1.3$, 1.5 or 1.7 is slightly lower than that for $\lambda = 1.0$ or 2.0 when $SFO = 0$ ppm. All the EVM values for $\lambda \geq 1.3$ are below -16.6 dB, which corresponds to a bit error rate of 10^{-3} for 16-QAM.

The EVM comparison between the 2nd, 3rd and 4th order polynomial interpolators is shown in Fig. 13(b). For $\lambda = 1.3$ the EVM with the 4th order interpolator is improved by ~ 0.5 dB (~ 1.5 dB) as compared with the 2nd (3rd) order interpolator, which is constant with the improvement in SINR in Fig. 8(b) and in EVM in Fig. 9(d). The relatively small improvement in EVM with the 4th order interpolator is observed in Fig. 13(c) when $\lambda = 2.0$. This can be explained by the fact that the SINR difference between the 4th and 2nd/3rd order interpolators becomes small for relatively high oversampling rate in Fig. 8(b). The EVM for $SFO \neq 0$ is almost equal to that for $SFO = 0$. The above experimental results agree very well with the numerical results. This confirms again that the proposed scheme of the SFO compensation using the 4th order interpolator can be used to effectively compensate a local oscillator frequency offset up to ± 1000 ppm in an OFDM-based VLC system with a minimum oversampling rate of 1.3 at the receiver.

V. CONCLUSION

Analytical study has been made of the combined LED nonlinear and aliasing effect during the digital process of the SFO compensation in an OFDM-based VLC system with practical LEDs. From the practical system design point of view, a 4th order piecewise polynomial interpolator using Farrow structure has been proposed to digitally compensate SFO between the transmitter and receiver oscillators. Based on a second-order polynomial nonlinear LED model, theoretical investigation has been conducted on the impact of both the LED nonlinearity and SFO-induced ICI on SINR of the received OFDM signal. With the optimized parameters for SFO estimation, it has been shown that the minimum required oversampling rate for achieving the maximum SINR using the 4th order interpolator is reduced

by approximately 15% and 50% in either the AWGN or VLC channel compared to the 2nd and 3rd order interpolators, respectively. Such an improvement can relax the sampling speed and accuracy requirement for DACs/ADCs. Both numerical and experiment results have shown that the proposed scheme can be used to effectively compensate a local oscillator frequency offset up to ± 1000 ppm at a minimum oversampling rate of 1.3 in an OFDM-based VLC system. The EVM with the 4th order interpolator is improved by ~ 0.5 dB (~ 1.5 dB) as compared with the 2nd (3rd) order interpolator.

REFERENCES

- [1] A. C. Boucouvalas, P. Chatzimisios, Z. Ghassemlooy, M. Uysal, and K. Yianopoulos, "Standards for indoor optical wireless communications," *IEEE Commun. Mag.*, vol. 53, no. 3, pp. 24–31, Mar. 2015.
- [2] A. V. N. Jalajakumari *et al.*, "High-speed integrated digital to light converter for short range visible light communication," *IEEE Photon. Technol. Lett.*, vol. 29, no. 1, pp. 118–121, Jan. 2017.
- [3] A. H. Azhar, T. A. Tran, and D. O'Brien, "A gigabit/s indoor wireless transmission using MIMO-OFDM visible-light communications," *IEEE Photon. Technol. Lett.*, vol. 25, no. 2, pp. 171–174, Jan. 2013.
- [4] H. Haas, "LiFi: Conceptions, misconceptions and opportunities," in *Proc. Int. Conf. IEEE Photon.*, Waikoloa, HI, USA, 2016, pp. 680–681.
- [5] H. Elgala, R. Mesleh, and H. Haas, "Indoor optical wireless communication: Potential and state-of-the-art," *IEEE Commun. Mag.*, vol. 49, no. 9, pp. 56–62, Sep. 2011.
- [6] H. Elgala, R. Mesleh, and H. Haas, "Indoor broadcasting via white LEDs and OFDM," *IEEE Trans. Consum. Electron.*, vol. 55, no. 3, pp. 1127–1134, Aug. 2009.
- [7] P. A. Haigh *et al.*, "Multi-band carrier-less amplitude and phase modulation for bandlimited visible light communications systems," *IEEE Wireless Commun. Mag.*, vol. 22, no. 2, pp. 46–53, Apr. 2015.
- [8] J. L. Wei, C. Sanchez, and E. Giacoumidis, "Fair comparison of complexity between a multi-band CAP and DMT for data center interconnects," *Opt. Lett.*, vol. 42, no. 19, pp. 3860–3863, Oct. 2017.
- [9] M. Speth, S. A. Fechtel, G. Fock, and H. Meyr, "Optimum receiver design for wireless broad-band systems using OFDM. I," *IEEE Trans. Commun.*, vol. 47, no. 11, pp. 1668–1677, Nov. 1999.
- [10] X. Wang, T. T. Tjhung, Y. Wu, and B. Caron, "SER performance evaluation and optimization of OFDM system with residual frequency and timing offsets from imperfect synchronization," *IEEE Trans. Broadcast.*, vol. 49, no. 2, pp. 170–177, Jun. 2003.
- [11] D. J. Foley and M. P. Flynn, "CMOS DLL-based 2-V 3.2-ps jitter 1-GHz clock synthesizer and temperature-compensated tunable oscillator," *IEEE J. Solid-State Circuits*, vol. 36, no. 3, pp. 417–423, Mar. 2001.
- [12] *Telecommunications and Information Exchange Between Systems-Part 11*, IEEE Standard 802.11a-1999, Dec. 1999.
- [13] M. Chen, J. He, Z. Cao, J. Tang, L. Chen, and X. Wu, "Symbol synchronization and sampling frequency synchronization techniques in real-time DDO-OFDM systems," *Opt. Commun.*, vol. 326, pp. 80–87, Sep. 2014.
- [14] H. Lee and J. Lee, "Joint clock and frequency synchronization for OFDM-based cellular systems," *IEEE Signal Process. Lett.*, vol. 18, no. 12, pp. 757–760, Dec. 2011.

- [15] M. F. Rabbi and C. C. Ko, "Timing jitter tracking for orthogonal frequency division multiple access system in high Doppler spread," *IET Commun.*, vol. 6, no. 11, pp. 1438–1446, Jul. 2012.
- [16] X. Q. Jin and J. M. Tang, "Optical OFDM synchronization with symbol timing offset and sampling clock offset compensation in real-time IMDD systems," *IEEE Photon. J.*, vol. 3, no. 2, pp. 187–196, Apr. 2011.
- [17] B. Ai, Z. Yang, C. Pan, J. Ge, Y. Wang, and Z. Lu, "On the synchronization techniques for wireless OFDM systems," *IEEE Trans. Broadcast.*, vol. 52, no. 2, pp. 236–244, Jun. 2006.
- [18] R. P. Giddings and J. M. Tang, "Experimental demonstration and optimisation of a synchronous clock recovery technique for real-time end-to-end optical OFDM transmission at 11.25 Gb/s over 25km SSMF," *Opt. Express*, vol. 19, no. 3, pp. 2831–2845, Jan. 2011.
- [19] M. Zhu, N. Cvijetic, M. F. Huang, T. Wang, and G. K. Chang, "Low-latency synchronous clock distribution and recovery for DWDM-OFDMA-based optical mobile backhaul," *J. Lightw. Technol.*, vol. 32, no. 10, pp. 2012–2018, May 2014.
- [20] Y. Cai *et al.*, "An effective sampling clock synchronization method for continuous- and burst-mode transmission in OFDMA-PONs," *Opt. Commun.*, vol. 384, pp. 78–84, Feb. 2017.
- [21] Z. Zhang, Q. Zhang, Y. Li, Y. Song, J. Zhang, and J. Chen, "A single pilot subcarrier-based sampling frequency offset estimation and compensation algorithm for optical IMDD OFDM systems," *IEEE Photon. J.*, vol. 8, no. 5, pp. 1–9, Oct. 2016.
- [22] Z. Zhang, Q. Zhang, J. Chen, Y. Li, and Y. Song, "Low-complexity joint symbol synchronization and sampling frequency offset estimation scheme for optical IMDD OFDM systems," *Opt. Express*, vol. 24, no. 12, pp. 12577–12587, Jun. 2016.
- [23] M. Chen, J. He, J. Tang, and L. Chen, "Pilot-aided sampling frequency offset estimation and compensation using DSP technique in DD-OOFDM systems," *Opt. Fiber Technol.*, vol. 20, no. 3, pp. 268–273, Jun. 2014.
- [24] R. Deng, J. He, M. Chen, and L. Chen, "SFO compensation by pilot-aided channel estimation for real-time DDO-OFDM system," *Opt. Commun.*, vol. 355, pp. 172–176, Nov. 2015.
- [25] H. Shafiee, B. Nourani, and M. Khoshgard, "Estimation and compensation of frequency offset in DAC/ADC clocks in OFDM systems," in *Proc. Int. Conf. IEEE Commun.*, Paris, France, 2004, pp. 2397–2401.
- [26] R. Deng, J. He, M. Chen, Y. Wei, J. Shi, and L. Chen, "Real-time VLLC-OFDM HD-SDI video transmission system with TS-based SFO estimation," in *Proc. Int. Conf. Opt. Fiber Commun.*, Los Angeles, CA, USA, 2017, pp. 1–3.
- [27] T. Pollet, P. Spruyt, and M. Moeneclaey, "The BER performance of OFDM systems using non-synchronized sampling," in *Proc. Int. Conf. IEEE Global Commun.*, San Francisco, CA, USA, 1994, pp. 253–257.
- [28] B. Ai, Y. Shen, Z. D. Zhong, and B. H. Zhang, "Enhanced sampling clock offset correction based on time domain estimation scheme," *IEEE Trans. Consum. Electron.*, vol. 57, no. 2, pp. 696–704, May 2011.
- [29] B. Ghimire, I. Stefan, H. Elgala, and H. Haas, "Time and frequency synchronisation in optical wireless OFDM networks," in *Proc. 22nd Int. Symp. IEEE Pers., Indoor, Mobile Radio Commun.*, Toronto, ON, Canada, 2011, pp. 819–823.
- [30] Y. Jiang, Y. Wang, P. Cao, M. Safari, J. Thompson, and H. Haas, "Robust and low-complexity timing synchronization for DCO-OFDM LiFi systems," *IEEE J. Sel. Areas Commun.*, vol. 36, no. 1, pp. 53–65, Jan. 2018.
- [31] F. M. Gardner, "Interpolation in digital modems. I. fundamentals," *IEEE Trans. Commun.*, vol. 41, no. 3, pp. 501–507, Mar. 1993.
- [32] L. Erup, F. M. Gardner, and R. A. Harris, "Interpolation in digital modems. II. Implementation and performance," *IEEE Trans. Commun.*, vol. 41, no. 6, pp. 998–1008, Jun. 1993.
- [33] F. Harris, "Performance and design of Farrow filter used for arbitrary resampling," in *Proc. 13th Int. Conf. Digital Signal Process.*, Santorini, Greece, 1997, pp. 595–599.
- [34] I. Neokosmidis, T. Kamalakis, J. W. Walewski, B. Inan, and T. Sphicopoulos, "Impact of nonlinear LED transfer function on discrete multitone modulation: Analytical approach," *J. Lightw. Technol.*, vol. 27, no. 22, pp. 4970–4978, Nov. 2009.
- [35] A. M. Cailean, B. Cagneau, L. Chassagne, V. Popa, and M. Dimian, "Evaluation of the noise effects on visible light communications using Manchester and Miller coding," in *Proc. Int. Conf. Develop. App. Syst.*, Suceava, Romania, 2014, pp. 85–89.
- [36] R. Yang, X. Jin, M. Jin, and Z. Xu, "Experimental investigation of optical OFDMA for vehicular visible light communication" in *Proc. Eur. Conf. Opt. Commun.*, Gothenburg, Sweden, 2017, pp. 1–3.

Qingqing Hu received the B.E. degree from the Dalian University of Technology, Dalian, China, in 2016. She is currently working toward the M.S. degree with the University of Science and Technology of China, Hefei, China. Her research interests include synchronization, advanced modulation, and DSP for optical wireless communications.

Xianqing Jin received the Ph.D. degree in optical communications from Bangor University, Bangor, U.K., in 2010. His thesis was focused on the study of optical OFDM for next generation local area networks and access networks. From 2012 to 2015, he had been a Postdoctoral Researcher with the University of Oxford, studying about the spatial multiplexing over ring-core fibers for future ultrahigh-speed optical networks. In 2016, he joined the University of Science and Technology of China, and was selected into national "1000 talents program" for young professionals in China. He is currently a professor working on high-speed optical wireless/fiber communications. His research interests include topics in optical OFDM, spatial multiplexing, and real-time DSP and PAT. He has authored or coauthored more than 80 refereed papers, and holds two international patents. Dr. Jin was the recipient of the Honorary Research Fellow Award for his significant contribution to the work at the Bangor University, in 2018.

Zhengyuan Xu received the B.S. and M.S. degrees from Tsinghua University, Beijing, China, and the Ph.D. degree from the Stevens Institute of Technology, Hoboken, NJ, USA. He was a Tenured Full Professor with the University of California, Riverside, CA, USA, and later with Tsinghua University before he joined the University of Science and Technology of China. He was the Founding Director of the multicampus center for Ubiquitous Communication by Light, University of California, and the Founding Director of the Wireless-Optical Communications Key Laboratory, Chinese Academy of Sciences. He is entitled the "Thousands Talents Program" Expert of China, and the Chief Scientist of the National Key Basic Research Program of China. His research interests include optical wireless communications, mobile networking, wireless big data, ranging, and localization. He has published more than 300 international journal and conference papers, and coauthored a book titled *Visible Light Communications: Modulation and Signal Processing* published by Wiley-IEEE Press. He has been on the Elsevier annual list of the Most Cited Chinese Researchers since 2014, and received 5000+ citations according to Google Scholar. He has served as an Associate Editor for different IEEE/OSA journals and was a Founding Chair of the IEEE Workshop on Optical Wireless Communications in 2010.